In-Depth Comparison of an Industrially Extruded Powder and Ingot Al Alloys

David Bombač [1],* , **Peter Cvahte [2]** , **Martin Balog [3]** , **Goran Kugler [1]** and **Milan Terčelj [1],***

[1] Faculty of Natural Sciences and Engineering, University of Ljubljana, 1000 Ljubljana, Slovenia; goran.kugler@ntf.uni-lj.si

[2] Impol 2000 d.d., 2310 Slovenska Bistrica, Slovenia; Peter.cvahte@impol.si

[3] Institute of Materials and Machine Mechanics, The Slovak Academy of Sciences, 84513 Bratislava, Slovakia; ummsbama@savba.sk

* Correspondence: david.bombac@ntf.uni-lj.si (D.B.); milan.tercelj@ntf.uni-lj.si (M.T.);
Tel.: +386-1-200-04-54 (D.B.); +386-1-200-04-62 (M.T.)

Abstract: An industrial press was used to consolidate compacted aluminum powder with a nominal diameter in the range of 1 μm. Direct and indirect hot-extrusion processes were used, and suitable process parameters were determined from heating conditions, ram speeds and billet temperatures. For comparison, a direct-extrusion press for hot extrusion of a conventional aluminum alloy AA 1050 was used. The extruded Al powder showed better mechanical properties and showed a thermal stability of the mechanical properties after annealing treatments. To increase the theoretical density of the directly extruded Al powder, single-hit hot-compression tests were carried out. Activation energies for hot forming were calculated from hot-compression tests carried out in the temperature range 300–580 °C, at different strain rates. Processing maps were used to demonstrate safe hot-working conditions, to obtain an optimal microstructure after hot forming of extruded Al powder.

Keywords: aluminum powder; hot extrusion; hot compression; activation energy

1. Introduction

The increased demand for weight reduction in components used in the aerospace and automotive industries requires the development of ever stronger materials. Due to their low density, aluminum alloys reinforced with various particles have been developed for weight-critical applications, which have a better specific strength compared to the basic matrix material. However, when reinforcing particles are added to the base metal, the ductility of the composite material is significantly worse, although there are beneficial effects on specific strength and wear resistance [1–5]. The low ductility and manufacturing problems prevent a wider application of aluminum matrix composites (AMC) [6]. Different reinforcing particles as reinforcing media have been tried and tested in AMCs. The most common are SiC, Al_2O_3, AlN, TiC and other reinforcing particles [2–13]. Typically, different volume fractions of reinforcing particles have been tested by extrusion, rolling or isostatic horizontal pressing, or only reinforcing particles have been mixed with Al prior to casting or powder compaction, to improve relative density, hardness, microstructure, wear resistance and strength. For a detailed overview of aluminum reinforced composites, please refer to Reference [14].

The strengthening mechanisms in particle-reinforced AMC are based on Orowan strengthening; grain and substructure strengthening; quench hardening from the dislocations created to compensate for the difference in thermal expansion coefficient between the reinforcing particles and the matrix; and work hardening due to strain mismatch between the particles [15]. Experimental confirmation of this is available and indicates that for a fixed reinforcement particle, the yield strength increases with

decreasing particle size [16–18]. The highest contribution to strength in the case of AMC reinforced with added ceramic particles is the formation of geometrically necessary dislocations enhanced by differences in elastic moduli and coefficients of thermal expansion in Al-matrix and ceramic reinforcements [6,19]. However, these mismatches also cause high matrix hardening and thus low ductility of AMCs. To avoid this, mixtures of ultrafine grains and nanocrystalline Al matrices with or without reinforcing particles have been proposed. Promising Al powder metallurgy routes are in situ–formed matrix composites in which the Al powder grain is either oxidized to form an Al_2O_3 surface layer or nitrided to form an AlN surface layer [7,20,21]. AMCs reinforced with AlN have also been produced by ball milling in NH_3 atmosphere, where AlN can be introduced in higher contents and is present not only on the surface but also inside the grains [10].

The in situ–formed AMCs contain only a small amount of the Al_2O_3 phase (typically less than 3 vol.%), but this thin layer prevents grain growth during hot consolidation and is responsible for the excellent thermal stability of the mechanical properties of in situ–formed AMCs [8,22]. Strengthening mechanism in the in situ–formed AMCs is unique and is attributed to the fine Al_2O_3 dispersoids along the Al grain boundaries, which is similar to strengthening mechanism in the oxide dispersion strengthen materials. A network of Al_2O_3 particles results in an increased slip resistance due to high stress from a dislocation pile-up at the particle network. The Al_2O_3 particle network and low angle grain boundaries do not contribute significantly to strengthening via the Orowan mechanism at room temperature and a significant contribution is due to the grain boundary strengthening. A further effect of the Al_2O_3 particle network is stabilization of the Al grain structure and prevention of grain growth, which was confirmed after long annealing times at high temperatures [23].

In this paper an industrial hot-extrusion press was used to consolidate aluminum Al 1080 powder in the range of 1 μm. As previously reported, Al 1080 powder grains in green compacts were covered with the Al_2O_3 phase as thin film originating from powder atomization [8,13,22]. Direct and indirect-extrusion processes were used to hot extrude Al 1080 powder compacts into a rectangular profile. For both extrusion processes similar die openings were used and corresponding processing parameters are given. Differences in the extrusion process and mechanical properties obtained by the two presses were compared with the conventionally produced and direct extruded commercial aluminum AA 1050 alloy. The hot formability of the extruded profile and in the annealed condition was evaluated by a single-hit compression test with the aim of improving the density of the powdered material and selecting an optimum processing window for hot forming with the aid of processing maps (superimposed power dissipation efficiency maps and instability maps determined from data from single-hit hot-compression tests).

2. Materials and Methods

Micron range aluminum powder Al 1080 used in this study was prepared by gas atomization of a commercially pure aluminum (Al > 99.5 wt.%) in N_2 atmosphere. The chemical composition of the supplied powder was determined instantly after gas atomization with Perkin-Elmer ICP 5000 spectrometer (PerkinElmer Inc., Waltham, MA, USA) and is given in Table 1. Comparison was made to conventionally prepared aluminum billet AA 1050 with the chemical composition given in Table 1 and determined with Spectrolab LAVMC07A spectrometer (SPECTRO Analytical Instruments GmbH, Kleve, Germany). Al 1080 aluminum powder particles are basically monocrystalline with oxide layer encapsulating them. All oxygen was assumed to be in Al_2O_3 oxide layer on the grain surface only. Laser diffraction, using Sympatec HELOS (Sympatec GmbH, Clausthal-Zellerfeld, Germany), yielded a nominal diameter of supplied powder as $d_{50} = 1.31$ μm ($d_{10} = 0.66$ μm and $d_{90} = 2.51$ μm).

Prior to hot extrusion, Al 1080 loose powder was compacted, using rubber isostatic pressing (RIP) or cold isostatic pressing (CIP), at a pressure of 100 MPa. Archimedes method was used to determine relative density of RIP or CIP compacted powder, extruded profiles and compressed samples.

Table 1. Chemical composition of as-atomized Al1080 powder and as-cast A1050 ingot in wt.%.

Material	Si	Fe	Cu	Mg	Mn	O	Al
Al 1080	0.054	0.159	0.001	0.005	0.001	1.95	base
AA 1050	0.114	0.148	0.002	0.02	0.008	-	base

2.1. Industrial Hot Extrusion and Annealing Heat Treatments

To consolidate and increase density of prepared compacted powder green pellets, an industrial hot extrusion presses (Impol Group, Slovenska Bistrica, Slovenia) were used. Industrial tests were made on six prepared compacted billets with length of 500 mm. Half of billets was extruded on a 55 MN direct-extrusion press (VAI Clecim SA, Savigneux, France) and other half on a 35 MN indirect-extrusion press (SMS group GmbH, Düsseldorf, Germany). In the direct-extrusion process, the green pellet billet is placed into a press container and pushed by a ram. Before the material begins to flow out of the die opening, the billet is pressed against the container wall and later through the extrusion die. Due to the considerable friction between the container and the green pellet billet, higher forces are needed compared to indirect extrusion. In indirect extrusion or backward extrusion, the extrusion die at the front of the hollow ram is pressed against the green pellet billet, which is prevented from movement in the container with back plate. As there is therefore no relative movement between the billet and the container, indirect extrusion produces less friction compared to direct extrusion.

To prevent microstructural change of compacted billets during heating to the extrusion temperature all compacted powder billets were encapsulated in a container. The billet for the direct-extrusion press had a container diameter of 291 mm, and the dimeter of compacted powder inserted into the container was 282 mm. The billet was extruded into a flat bar, with nominal dimension of 95 mm × 40 mm, where die dimensions were 96.8 mm × 41.2 mm. Extrusion ratio for direct press was 17.5 based on the die and billet dimensions. AA 1050 billet made by using conventional metallurgy for comparison of properties was extruded, using the same die only with the 55 MN direct-extrusion press. All extrusion parameters used for direct extrusion are given in Table 2.

Table 2. Extrusion parameters used for 55 MN direct-extrusion press.

Billet Material	Al 1080 Powder			AA 1050
Billet Mark	D1	D2	D3	D4
Billet length/mm	500	500	500	700
Ram speed/mm·s^{-1}	3.5	2.1	1	5.7
Puller (bar) speed/m·s^{-1}	0.062	0.035	0.017	0.1
Peak press pressure/MPa	23	27.4	28.7	5.3
Press rest/mm	50	50	50	130
Die furnace temperature/°C	460	450	440	500
Container temperature/°C	450	450	450	450
Billet temperature/°C	460	450	445	460
Maximum bar temperature/°C	587	570	555	560

Technological parameters used for extrusion with 35 MN indirect press are listed in Table 3. Extruded product was a flat bar with nominal dimensions of 90 mm × 50 mm, where die opening had dimensions of 91.3 mm × 50.8 mm. Billet diameter for the indirect press was a bit smaller compared to one used with the direct press and had container diameter of 280 mm and compacted powder diameter of 274 mm. Extrusion ratio was 13.3 on the indirect press based on the die and billet dimensions.

Billets were for both extrusion presses heated, using indirect heating methods available in workshop for each extrusion press. A gas indirect-heating furnace was used to heat billets extruded with 55 MN direct-extrusion press. For 35 MN indirect-extrusion press electric indirect heating furnace (Impol Group, Slovenska Bistrica, Slovenia) was used to heat billets to the highest possible temperature of 340 °C. The idea was then to use separate induction furnace to heat billets to desired extrusion

temperature. However, during the first industrial test with indirect press it was found out during heating the billet marked I1 that time need to reach desired temperature of 420 °C from 340 °C was approximately 20 min. This was considered too long, especially when compared to conventionally cast AA 1050, where the time needed to increase temperature from 340 to 520 °C, using the same induction heating, is approximately 2 min. Therefore, decision was made to start extrusion of billets I2 and I3 with temperatures around 340 °C obtained solely with electric indirect heating furnace.

Table 3. Extrusion parameters used for 35 MN indirect-extrusion press.

Billet Material	Al 1080 Powder		
Billet Mark	I1	I2	I3
Billet length/mm	500	500	500
Ram speed/mm·s^{-1}	7.1	6.2	3.9
Puller (bar) speed/m·s^{-1}	0.118	0.082	0.052
Peak press pressure/MPa	17.7	20.5	21.4
Press rest/mm	50	50	50
Die furnace temperature/°C	340	340	320
Induction furnace temperature/°C	420	-	-
Container temperature/°C	360	360	360
Billet temperature/°C	420	340	320

Annealing heat treatment study was performed to investigate influence of temperature on obtained mechanical properties and recovery/recrystallization resistance at elevated temperatures. Annealing was performed in an industrial furnace at temperature of 300 °C for all samples. Annealing time was varied and selected annealing times were 1, 5, 9 and 20 h for extruded powder material and conventionally cast and extruded Al.

2.2. Hot Workability and Mechanical Properties

Mechanical properties were determined with tensile test at room temperature according to SIST EN 10002-1:2002 standard. Samples for tensile test were machined from the center of extruded bar with a diameter of 10 mm and gauge length of 50 mm. Tensile teste were carried out on a Zwick Z400 tensile tester (ZwickRoell AG, Ulm, Germany) with a strain rate of 4×10^{-4} s^{-1}.

Hot workability was investigated with a single-hit hot-compression tests performed on a Gleeble 1500D thermomechanical simulator (Dynamic Systems Inc., Poestenkill, NY, USA). Cylindrical specimens machined from extruded billets in non-annealed and annealed states with a diameter of 10 mm and length of 15 mm were used. True stress versus true strain curves were determined for experiments conducted for a range of strain rates between 0.1 and 10 s^{-1} (0.1, 1, 5 and 10), at temperatures between and 570 °C. Samples were heated to deformation temperature, with a heating rate of 1 °C·s^{-1}. Samples held at the deformation temperature for 60 s and then compressed. To reduce friction and avoid inhomogeneous deformation, Ta foils with 0.05 mm in thickness, and graphite foils were inserted between the cylindrical specimen and the compression tool. After deformation samples were quenched to preserve microstructure of hot compressed samples.

2.3. Microstructural Characterization

Microstructure of conventional AA 1050 Al was characterized with light optical microscopy, using Leica MEF4 microscope (Leica Microsystems GmbH, Wetzlar, Germany) in polarized light. Samples were prepared by conventional metallography and electrolytic etching in 2.5 vol.% HBF$_4$ aqueous solution for 90 s at 25 V. Al 1080 powder was characterized by using scanning electron microscopy (SEM, JEOL Ltd., Tokyo, Japan) with JEOL JSM-7600F and transmission electron microscopy (TEM, JEOL Ltd., Tokyo, Japan) with JEOL JEM-100C electron microscope operated at 100 kV. TEM samples were polished electrolytically, using 10 vol.% perchloric acid, 10 vol.% ethyleneglycol and 80 vol.% ethanol, at −50 °C.

3. Results

3.1. Microstructure
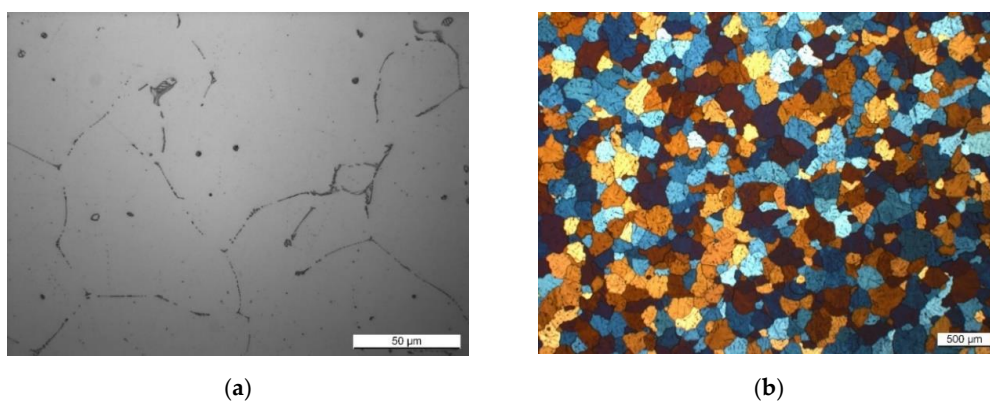
3.1.1. Initial Microstructure

Electron microscopy micrographs (SEM and bright field TEM) of Al 1080 powder are shown in Figure 1. Figure 1a depicts secondary electron SEM micrograph of a micron range loose powder. Figure 1b shows a bright field TEM micrograph of compacted powder after CIP (green pellet) with marked Al_2O_3 grain surface film. In Figure 1b an aluminum oxide (Al_2O_3) layer is visible on the powder grain surfaces (marked with arrows). The powder particles are monocrystalline with only a few dislocations after CIP. For a more detailed characterization of the same Al 1080 powder as the powder used in the current study, see Reference [22], where selective area diffraction was used to prove that the oxide layer on the grains is Al_2O_3.

(a)

(b)
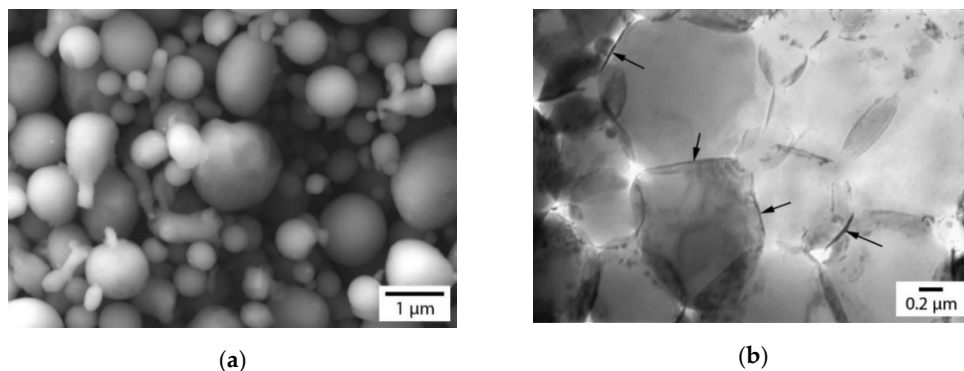
Figure 1. Electron microscopy micrographs of Al 1080 powder: (**a**) loose micron range powder (SEM); (**b**) compacted Al 1080 powder, using cold isostatic pressing (CIP) at 100 MPa (bright field TEM).

High plastic deformation capabilities of loose Al 1080 powder were expected due to only few observed dislocations in TEM micrographs. Density of compacted powder (green pellet) as determined with Archimedes method reached 85% density of an ideal Al density (2.7 g·cm^{-3}). An aluminum oxide Al_2O_3 phase present on the powder particle boundaries have higher density (3.66 g·cm^{-3}) compared to an ideal Al. However, due to estimated small amount of Al_2O_3 phase it was neglected in determination of the density.

Conventionally prepared AA 1050 alloy is not comparable in the size of grains to powder metallurgy route, with its average grain size around 100 μm. Figure 2 show initial microstructure of cast and homogenized AA 1050 before extrusion.

(a)

(b)

Figure 2. Initial microstructure of cast and homogenized AA 1050: (**a**) etched in Nital (2 vol.%); (**b**) micrograph taken in polarized light.

3.1.2. Microstructure after Extrusion

Bright field TEM micrographs of extruded Al 1080 powder are shown in Figure 3. The micrograph shown in Figure 3a was taken from a profile extruded by indirect extrusion and shows that the grain size did not change significantly after extrusion. The Al_2O_3 layer was only slightly deformed after extrusion (see Figure 3a), indicating that grain growth was inhibited. Due to the higher extrusion ratio in direct extrusion, a higher deformation of the powder particles was expected. As shown in Figure 3b, significant grain elongation and damage to the surface oxide layer occurred after direct extrusion. The measured density of the extruded Al 1080 powder in both cases was about 95% of the theoretical pure Al density. In order to further improve the density of the material after extrusion, subsequent hot forming is necessary.

(**a**)　　　　　　　　　　　　　　　　　　　　　（**b**)
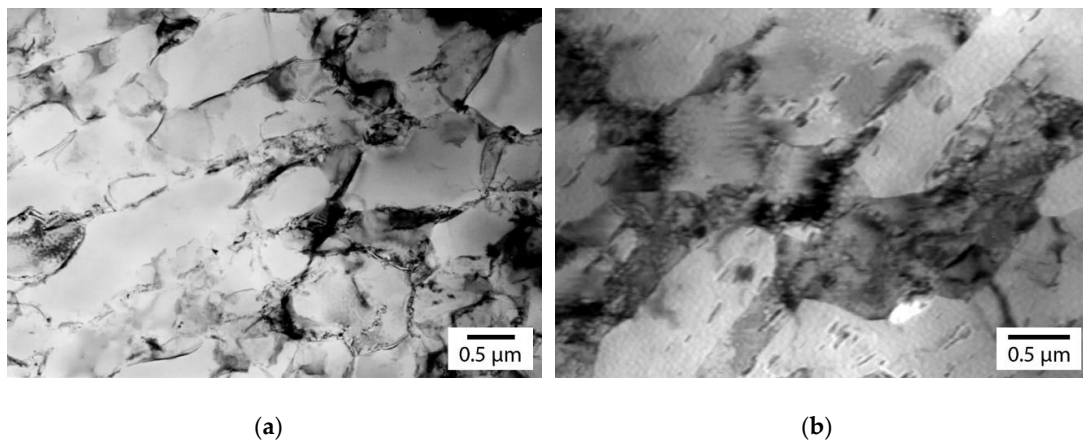
Figure 3. Bright field TEM micrographs of Al 1080 powder after extrusion (longitudinal direction): (**a**) direct extrusion and (**b**) indirect extrusion.

The microstructure of conventional AA 1050 Al is, again, not comparable in grain size to the powder metallurgy route and is shown in Figure 4. The micrograph of an extruded AA 1050 profile is shown in Figure 4a, where the typical extrusion texture with small, elongated grains and with some large recrystallized grains embedded in the microstructure can be seen. After annealing heat treatment, the number of large recrystallized grains increases, as shown in Figure 4b.


(**a**)　　　　　　　　　　　　　　　　　　　　　（**b**)
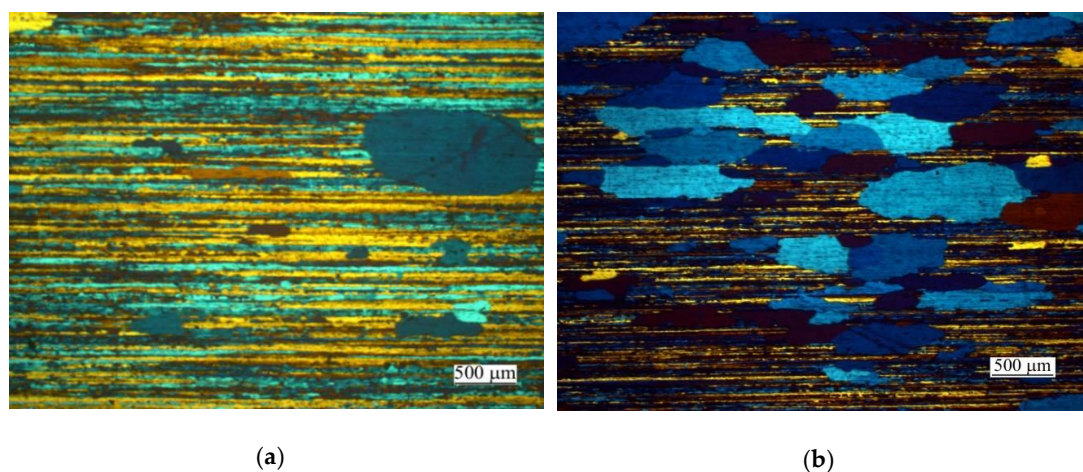
Figure 4. Polarized light optical micrograph of AA 1050 after (**a**) direct extrusion and (**b**) annealing for 20 h, at 300 °C, following direct extrusion.

3.2. Industrial Hot-Extrusion Tests

3.2.1. Direct-Extrusion Press

Three Al 1080 powder billets (green pellets), heated to different temperatures and using different ram speeds, were extruded into a rectangular profile. After extruding the Al 1080 billets, a single conventional aluminum metallurgy AA 1050 billet was extruded by using the same die. The pressures achieved in the main cylinder of the direct press applicable to all four extruded billets are shown in Figure 5. In addition, Figure 5 also shows the temperature measured on the extruded profiles immediately after leaving the die during direct extrusion, which was measured between 512 and 587 °C. Due to the temperature measurement at the exit from the die, there is a time delay after the peak pressure.
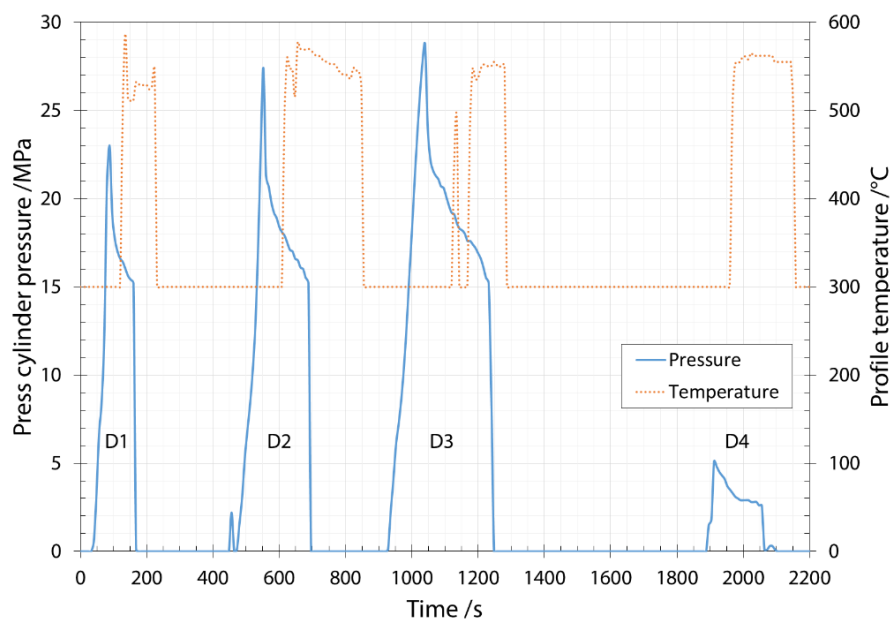
Figure 5. Main cylinder pressure and measured extruded profile temperature for all billets extruded with direct-extrusion press. Details of process parameters are listed in Table 2.

As expected, the pressure in the main cylinder increases with lower billet temperature. The lowest pressure in the extrusion press cylinder was reached during the extrusion of billet D1, which had the highest ram speed of all three powdered billets. Although billet D3 was extruded with the peak cylinder pressure close to the capabilities of the press (30 MPa), the surface quality of the extruded profile was better than the surface quality of billets D1 and D2, where surface cracks were observed. Therefore, the most suitable ram speed for direct extrusion of Al 1080 powder in the micron range was determined to be 1 mm·s^{-1}. The maximum measured profile temperature is the highest for extruded billet D1 and was measured at 587 °C. The powder billet D3 had the lowest measured extrusion profile temperature at 555 °C. Although the maximum measured profile temperatures were significantly different for all three extruded powder billets, the average temperature throughout the extrusion process was similar and was calculated at about 542 °C and was lower than average temperature of the billet D4, where it was calculated at about 554 °C.

A comparison between extrusion of Al 1080 powder and conventionally cast and homogenized AA 1050 billets of comparable chemical composition showed that the peak cylinder pressure for AA 1050 billet was about 5 MPa and was about five times lower than the peak pressures achieved in the extrusion of Al 1080 powder. Part of the difference in cylinder pressures can be attributed to differences in grain size, and part to the porosities present in the compacted powder green pellet, which cause a significant increase in friction and resistance to continuous material flow. The latter is confirmed by a

significant increase in pressure at the beginning of the extrusion of Al 1080 powder, which decreases rapidly after the initial spike. Material flow instabilities, which are influenced by the oxide layer surrounding each powder particle, are another reason for much higher cylinder pressures, which could also be attributed to large profile temperature variations. The D4 billet had a peak cylinder pressure that was much lower than the average extrusion pressure, and the measured temperature of the extruded profile is very stable.

3.2.2. Indirect-Extrusion Press

Pressures reached in the main cylinder during indirect extrusion, shown in Figure 6, apply to all three extruded profiles. The maximum allowable pressure at indirect press is 25 MPa, and the values achieved during extrusion were significantly lower for all three extruded profiles. Due to the lower billet temperatures, the ram speeds were different for all three extruded profiles. Profile I1 was extruded at 418 °C, and the ram speed achieved was 7.1 mm·s^{-1}, with a peak pressure of 17.7 MPa. Using a die with an extrusion ratio of 13.3 for the extrusion of square profiles resulted in a profile with cracked edges. Similarly, cracked edges were obtained when the ram speed was reduced to 6.2 mm·s^{-1} during the extrusion of profile I2, where the billet was heated to 340 °C. In this case, the peak cylinder pressure reached 20.5 MPa. During extrusion of profile I3, the ram speed was reduced to 3.9 mm·s^{-1}. In the latter case, the temperature of the billet was 320 °C, and the peak pressure reached 21.4 MPa, while no edge cracks were observed. Since the die was pressed into the billet with a hollow ram, the temperature at the exit of the die could not be measured.
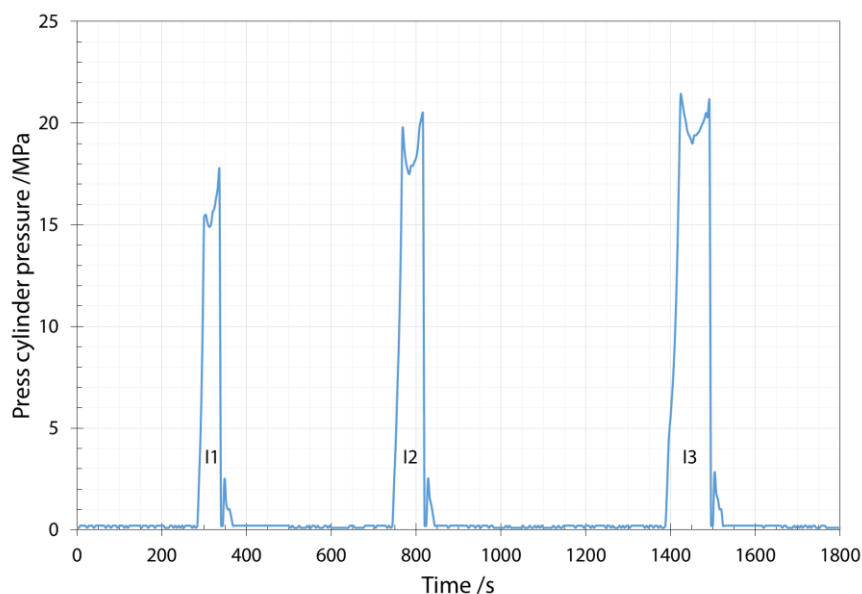

Figure 6. Main cylinder pressure for all billets extruded with indirect-extrusion press (details listed in Table 3).

3.3. Mechanical Properties of Extruded Material

The mechanical properties achieved by Al 1080 after extrusion and in the annealed state after 20 h at 300 °C are shown in Figure 7. The comparison is made for direct and indirect extruded profiles and for extruded conventional AA 1050 alloy in the as-extruded and in the annealed condition. After 20 h annealing at 300 °C, a slight drop in ultimate tensile strength (UTS) and yield stress (YTS) was measured. The highest tensile strength and the highest yield strength were achieved in the sample extruded with direct press. However, ductility in this sample was the lowest. Achieved strain at fracture in the sample produced by indirect press was more than twice as high compared to the sample extruded by direct press. While UTS and YTS from the direct press were close together, the behavior of the sample extruded with indirect press was more comparable to conventionally cast and extruded

AA 1050 alloy. The lowest UTS and YTS values were obtained with the conventionally cast and direct extruded AA 1050 specimen, while ductility of this specimen was the highest. In the tempered AA 1050 specimen, strain at fracture increased by about 6%, as compared to the untempered state. In the powdered Al 1080 specimen extruded by direct press, the increase in strain was about 2%, while in the specimen extruded by indirect press, only 0.5% increase in strain was obtained.
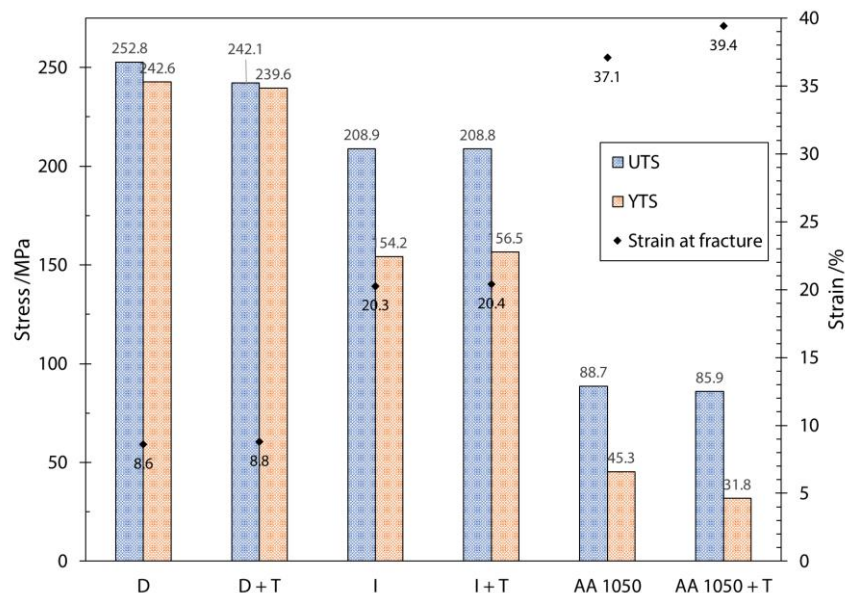
Figure 7. Summary of mechanical properties for extruded and for 20 h at 300 °C annealed materials. Where D is direct press extruded, and D + T is direct press extruded and for 20 h at 300 °C annealed sample; I is indirect press extruded sample; I + T is indirect press and for 20 h at 300 °C annealed sample and similarly for direct-press-extruded AA 1050 Al, and the same also for 20 h at 300 °C annealed AA 1050 sample.

3.4. Hot-Compression Tests

Single-hit hot-compression tests were carried out to investigate the material behavior at elevated temperatures, in order to determine a suitable hot forming window and to further increase the density of the extruded Al 1080 powder. The decision to use hot-compression tests also made it possible to simulate forging of extruded Al 1080 powder. The measured density of the extruded Al 1080 specimen after hot-compression test reached 99.98% of the theoretical value. Several strain rates were used, and the true stress versus true strain curves shown in Figure 8 were obtained. At low strain rates (0.01 and 0.1 s^{-1}), cracking occurred on the specimen surface. This is shown in Figure 8a, where an unstable material flow at true strains of about 0.4 is shown for the strain rate of 0.1 s^{-1}. The flow curves during single-hit hot compression of the directly extruded specimens are shown in Figure 8, compared to the extruded AA 1050 alloy. No surface cracks were observed in the AA 1050 specimens at all temperatures and strain rates used. In addition, AA 1050 shows typical dynamic recovery (DRV) behavior, and peak stress values are many times lower (from about three to seven times), depending on the deformation temperature compared to extruded Al 1080 powder.

(**a**)

(**b**)

(**c**)

(**d**)

(**e**)

(**f**)
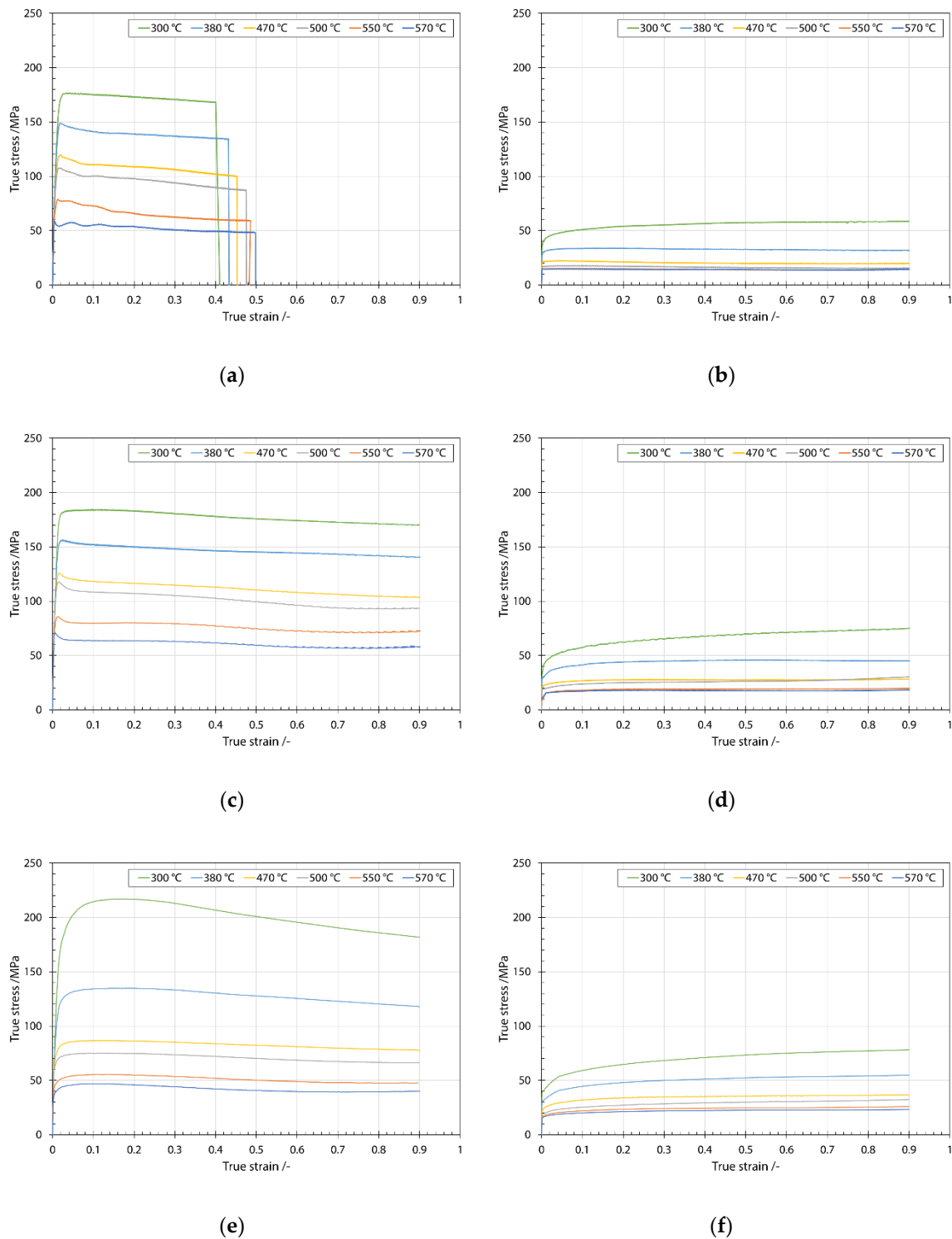
Figure 8. Single-hit hot-compression flow curves at various temperatures: (**a**) directly extruded Al 1080 powder, at a strain rate of 0.1 s^{-1}; (**b**) directly extruded conventional AA 1050 alloy, at a strain rate of 0.1 s^{-1}; (**c**) directly extruded Al 1080 powder, at a strain rate of 1 s^{-1}; (**d**) directly extruded conventional AA 1050 alloy, at a strain rate of 1 s^{-1}; (**e**) directly extruded Al 1080 powder, at a strain rate of 5 s^{-1}; and (**f**) directly extruded conventional AA 1050 alloy, at a strain rate of 5 s^{-1}.

The values for the peak stresses in single-hit-hot-compression tests were collected for all deformation conditions and are shown in Figure 9. As expected, a clear trend of decreasing peak stress

with increasing temperature can be seen, and with increasing strain rate, peak stress values increase at any temperature. The collected values for extruded Al 1080 powder and conventionally produced AA 1050 alloy were used to determine the activation energies for hot deformation, using the following Zener–Hollomon parameter and the hyperbolic sine equation [24–26]:

$$Z = \dot{\varepsilon} \, \exp\left(\frac{Q}{RT}\right) = A \sin h^n(\alpha\sigma), \tag{1}$$

where Z is the Zener–Hollomon parameter; R is the gas constant; Q is the apparent activation energy for hot deformation; and A, n, and α are material constants. Details of the minimization procedure and how the parameters are determined are given elsewhere [25,26]. Figure 9 shows the relationship between peak stress and temperature along the experimental peak stresses described by a hyperbolic sine function, using Equation (1). A good agreement was obtained between the calculated hyperbolic sine function of the Zener–Hollomon parameter and the experimental values.


(a)　　　　　　　　　　　　　　　　　　　　　　　(b)
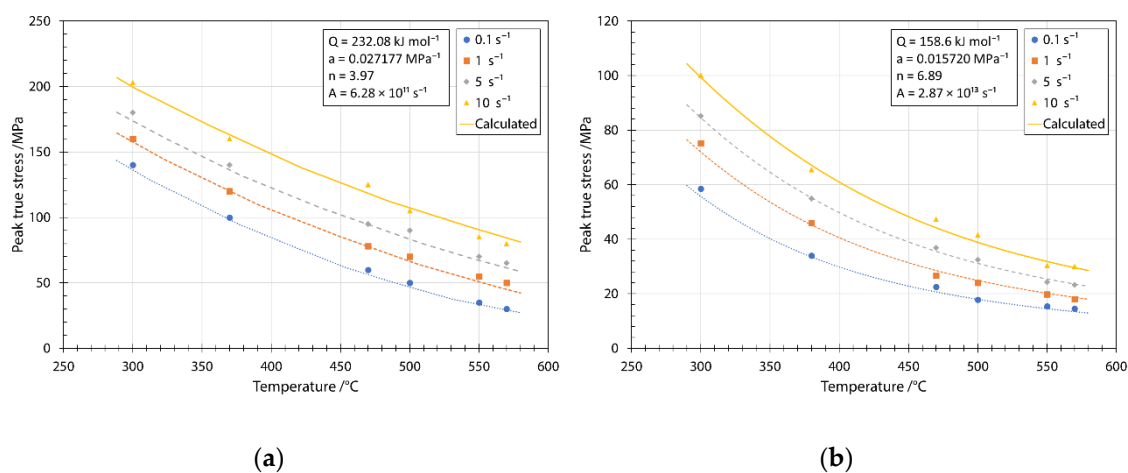
Figure 9. Temperature dependence of an experimental and calculated peak true stress values for various strain rates: (**a**) direct press extruded Al 1080 powder and (**b**) conventional direct press extruded aluminum AA 1050 alloy.

Single-hit hot-compression tests were performed not only on extruded material but also on samples subjected to annealing heat treatment. Flow curves obtained at a strain rate of 5 s^{-1} for a given material and different annealing times are shown in Figure 10. It can be seen that extruded conventional AA 1050 alloy behaves similarly to the extruded Al 1080 powder, where the activation energy for deformation increases after annealing at 300 °C for 1 h. In both cases, the activation energy for deformation decreases after 20 h annealing at 300 °C. The activation energy for deformation in extruded AA 1050 alloy is close to the activation energy of Al self-diffusion (144.4 kJ·mol^{-1} in the Al single crystals [27]), the differences in both being due to the fine grains obtained after extrusion (see Table 4).

Table 4. Comparison of apparent activation energies for hot deformation and material parameters for extruded and annealed conditions for Al 1080 powder and conventional AA 1050 alloy.

Material	Annealing Time/h	Q/kJ·mol^{-1}	α/MPa^{-1}	n/-	A/s^{-1}
Al 1080 powder	As extruded	232.08	0.027177	3.97	6.28×10^{11}
	1	252.5	0.028282	4.25	1.81×10^{15}
	20	209.7	0.025506	3.99	9.03×10^{12}
Conventional AA 1050	As extruded	158.6	0.01572	6.89	2.87×10^{13}
	1	165.1	0.023924	6.28	1.90×10^{12}
	20	154.0	0.023347	6.18	4.02×10^{11}

(**a**)　　　　　　　　　　　　　　　　　　　　(**b**)
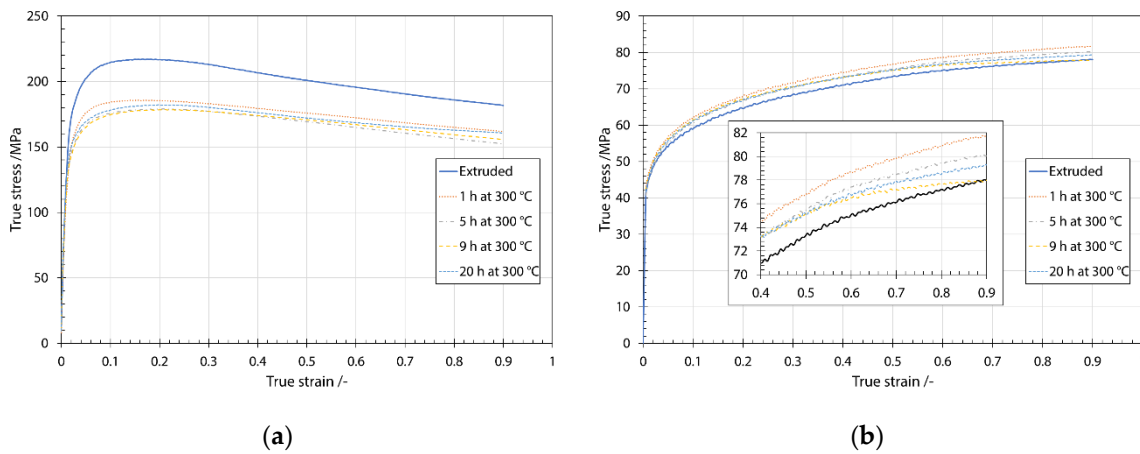
Figure 10. Influence of annealing time, at a temperature of 300 °C, on flow curves from a single-hit hot-compression test, at a strain rate of 5 s^{-1}: (**a**) directly extruded Al 1080 powder and (**b**) conventional directly extruded AA 1050 alloy.

The influence of the annealing time at an annealing temperature of 300 °C on the obtained hot-compression flow curves, at a strain rate of 5 s^{-1}, is shown in Figure 10. A comparison is made with the flow curves for extruded Al 1080 powder and conventionally cast AA 1050 alloy. For Al 1080 powder, even after a short annealing time of 1 h, a greater deviation from the flow curve of as extruded material was obtained, while the curve shapes are remarkably similar in all cases. In the case of Al 1080 powder, the deformation behavior is virtually unchanged at annealing times of 5 h or more (see Figure 10a). Alloy AA 1050 shows virtually unchanged flow behavior independent of annealing time, and the detailed flow curve at true strains between 0.4 and 0.7 is shown in Figure 10b in the sectional view.

Processing Maps

The best hot-forming conditions for directly extruded Al 1080 powder material were determined by means of processing maps based on the dynamic material model. For further details on the basis of the processing maps, please refer to References [28,29]. The processing maps shown in Figure 11 for strains 0.1, 0.2, 0.4 and 0.6 as an overlay of the contour map in percent, which represents the power dissipation efficiency, and the flow instability map, which is shown as darkened areas.

(**a**)　　　　　　　　　　　　　　　　　　　　(**b**)

Figure 11. *Cont.*

(**c**)　　　　　　　　　　　　　　　　　　　　　(**d**)
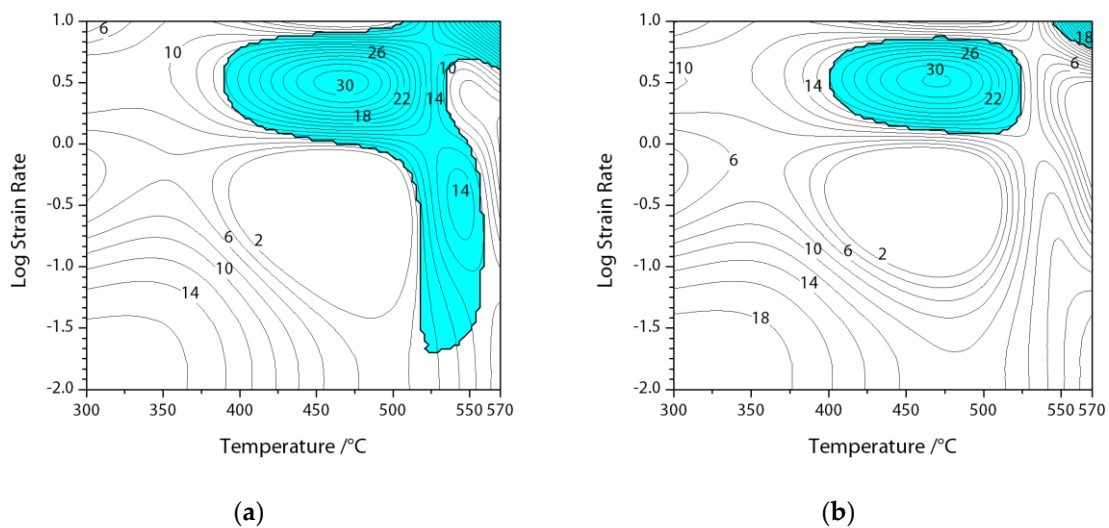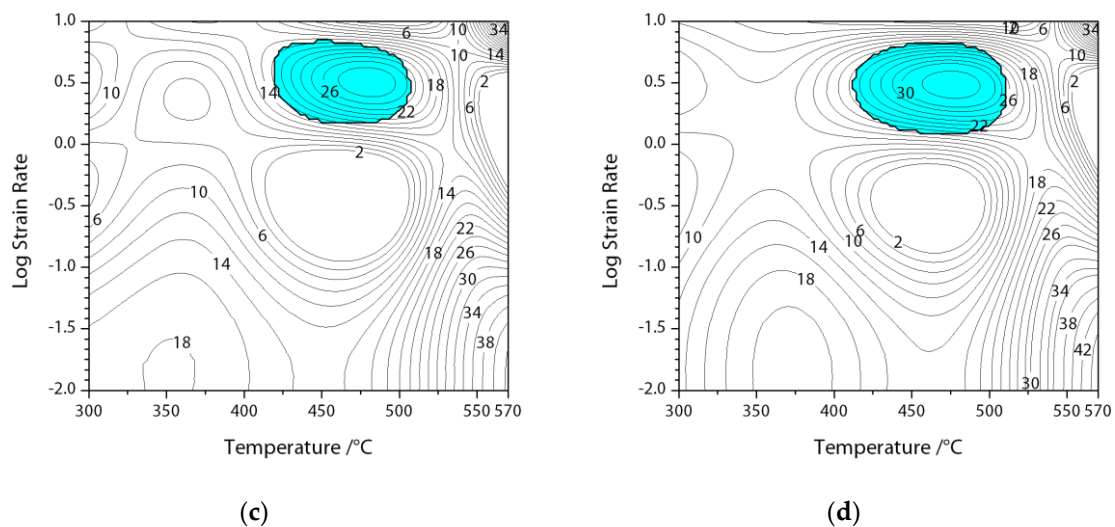
Figure 11. Processing maps based on the dynamic material model for Al 1080 powder extruded with direct press: (**a**) at strain 0.1, (**b**) at strain 0.2, (**c**) at strain 0.3 and (**d**) at strain 0.6.

Flow instabilities during hot forming of directly extruded Al 1080 powder are concentrated at low strain rates and temperatures above 400 °C. At strains greater than 0.2, the unstable flow area moves to higher strain rates and concentrates in the temperature window between 400 and 500 °C.

4. Discussion

To convert loose Al powder into usable bulk material, industrial hot extrusion was carried out at various temperatures and extrusion speeds. Direct and indirect extrusion was used, which allowed us to determine differences in mechanical properties and to optimize the appropriate powder processing route and parameters. Green pellets were first extruded with an indirect press, as lower pressure and energy consumption is required compared to direct extrusion. As the material flow is different for both types of extrusion processes, better results were expected when using the indirect press compared to the direct-extrusion press. However, the oxide present on the powder grains affected heating in an industrial environment and similar final extrusion densities were obtained after both types of extrusion. As the density reaches about 95% of the theoretical density, subsequent hot forming is necessary to improve the density of the powder material after extrusion. Direct extrusion was used to produce profiles from AA 1050 Al alloy produced by conventional casting and the results obtained were compared. The processing routes for Al powder and conventional metallurgy are shown schematically in Figure 12.

A better tensile strength of the extruded Al powder was achieved by direct extrusion (see Figure 7). During extrusion, an oxide layer present on the powder grains is damaged. This leads to the rearrangement and rotation of some grains due to deformation gradients. Later annealing studies showed that extruded Al powder is not significantly affected by annealing at 300 °C even after 20 h. During annealing of the extruded material, the process of partial polygonization begins in agreement with processes that occur in extruded Al alloys. This phenomenon can be confirmed by changes in the calculated activation energy for hot deformation at different annealing times and in the extruded state, although the grain size was not measured.

To increase the density of the extruded Al powder, a further hot deformation process is proposed. The investigation of hot forming of extruded and annealed material with a single-hit compression test showed that the shapes of the flow curves obtained after different annealing times are similar to those of extruded material. However, in general, the yield stress values are about 15% lower even after 1 h of annealing. It is expected that the material has become stable as grain growth is prevented by the oxide surrounding the individual powder grains. Calculated processing maps based on the

dynamic material model (superimposed maps of power dissipation efficiency and flow instability) show unstable areas at low strain rates consistent with single-hit hot-compression tests. Under these conditions, wedge cracks are typical when grain boundary sliding due to shear stresses causes wedge cracks on triple junctions to reduce stress concentration [28]. Flow instabilities are not present at higher strain rates and lower temperatures. Optimum hot forming conditions based on the processing maps are for strains 0.4 and 0.6 at temperatures above 550 °C and strain rates above 1 s^{-1}. From a practical point of view, the experimental results from this work can be applied to the hot forming process of extruded aluminum powder with Al_2O_3 layer on the grain surfaces.
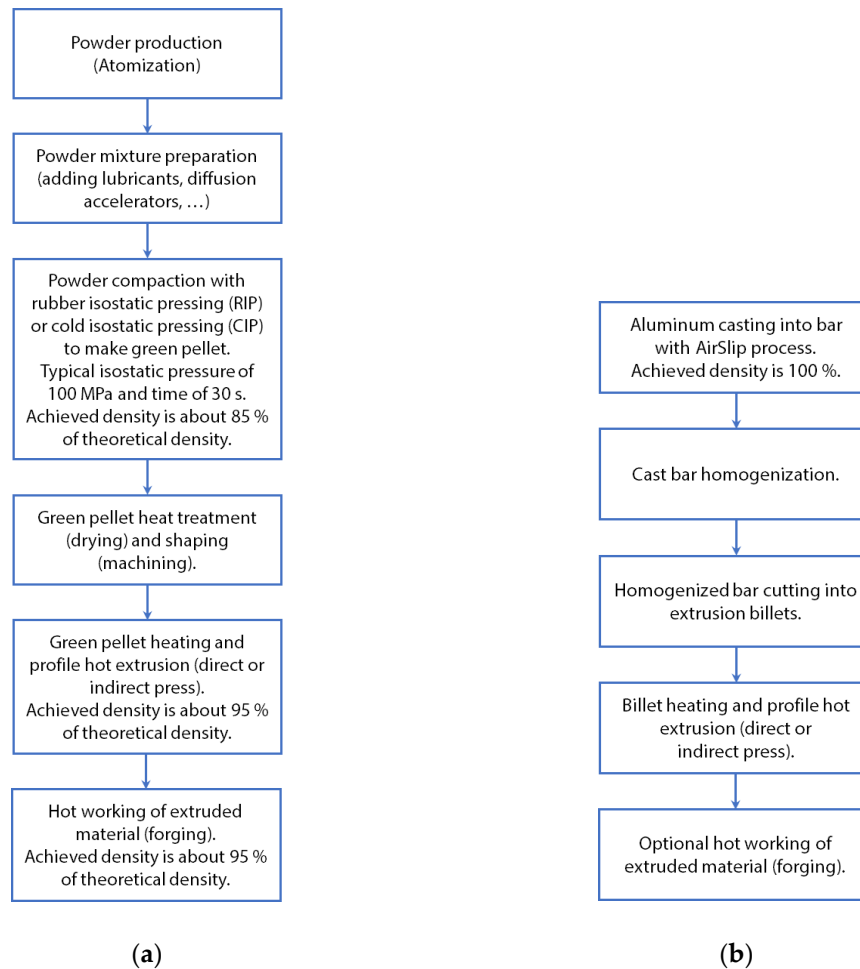
Figure 12. Technology and process routes for (**a**) Al 1080 powder and (**b**) conventional AA 1050 alloy.

Table 5 lists the results of mechanical properties of aluminum composites at room temperature, available in the literature, along with the results of as-extruded material from the current study. Compared to the present study, in which ultrafine powder grains without additionally added particles were used, a study by Kubota [30] used a relatively large Al grains (100 μm). Similar to the present study, Kubota used γ-Al_2O_3-matrix-reinforced Al and achieved comparable values of UTS to the present study. However, Kubota did not specify the gauge length of the tensile specimens used. In a study by Gubicza et al. [31], using a mixture of large grain (1–10 μm) and ultra-fine grain (100 nm) Al, they obtained UTS about two times higher, as compared to the present study, with better ductility. Shi et al. [1] extruded ultra-fine air atomized Al-4Y-4Ni and Al-4Y-4Ni-0.9Fe (in at.%), with UTS as 422 and 478 MPa measured at room temperature, YTS measured as 394 and 470 MPa, while strain at failure was determined as 16.3 and 7.2%, respectively. It should be noted that they used specimens with a very small gauge length (only 1.3 mm), which resulted in higher reported values. Extruded

Al powder reinforced with different graphite contents was investigated by Flores-Zamora et al. [3]. They achieved better mechanical properties with added graphite, but similar to the present study, the ductility was lower with increased graphite content. The mechanical properties were determined according to ASTM standard, with measured YTS values from 147 to 164 MPa, and UTS from 176 to 199 MPa. Similar tensile strengths and strains were also determined by Zhang et al. [32] (Al-10 wt.% Mg powders (100 μm)), Song and He [33] (Al powder (40 μm) and 20 vol.% SiC powder (70 μm) mixture after extrusion), and Kennedy and Wyatt [4] (Al powder with 10 vol.% TiC (10 μm)). In our case, the value obtained for the tensile strength was 253 MPa, while the elongation reached the value of 8.6%. Fan et al. [9] examined the extruded, cryomilled Al-Mg (7.5 wt.% Mg) alloy. They performed only one pressure study and achieved the strength of their material at 600 MPa. In the case of Choi et al. [34], nanocrystalline Al with a grain size of 48 nm showed UTS at 500 MPa and an elongation of about 1%. As the grain size increased to 72 nm, the value of UTS dropped to 279 MPa, while the elongation was 5%. Table 5 shows not only the results of the powder route, but also the published results of Al-composite materials reinforced with cast particles [35–37]. The reinforcing particles used in these studies were Bi_2O_3 coated $Al_{18}B_4O_{33}$ [35], SiC [36] and Al_2O_3 [37]. The tensile strength values obtained were in the range of 302–641 MPa, while elongation was in the range 0.5–8.8%.

Table 5. Comparison of published room-temperature yield tensile strength, ultimate tensile strength and strains at fracture for various particle reinforced aluminum composites.

Material	YTS/MPa	UTS/MPa	Strain/%	Reference
Al-4Y-4Ni (ultra-fine grains)	394	422	16.3	[2]
Al-4Y-4Ni-0.9Fe (ultra-fine grains)	470	478	7.2	
Al-graphite (0.5 wt.%) composite	147	176	25	[3]
Al-graphite (1 wt.%) composite	164	199	22	
Al powder + 10 vol.% TiC (10 μm)		129	32	[4]
Air atomized pure Al (100 μm) + γ-Al_2O_3 in matrix		288		[30]
Mixture of large (1–10 μm) and ultra-fine (100 nm) Al grains	390 +	480 +	17	[31]
Al powder (40 μm) + 20 vol.% SiC (70 μm)	117	146	9.6	[33]
Al + 10 wt.% Mg powders (100 μm)	137	147	7	[32]
Pure Al + Bi_2O_3 coated $Al_{18}B_4O_{33}$ whiskers composite		302	8.8	[35]
Ultrafine Al-Mg (7.5 wt.%) grains (120 nm)		600 +	0.2–0.4 ‡	[38]
AA 2214 + 26 wt.% SiC (3 μm) − forged	290	446	3.1	[36]
AA 2214 + SiC (26 wt.%) − forged + T4	451	641	2.5	
Nanocrystalline bulk Al (48 nm)		500	1	
Nanocrystalline bulk Al (56 nm)		460	3	[34]
Nanocrystalline bulk Al (72 nm)		279	5	
AA 2618 + Al_2O_3 (20 vol.%)–as-cast	347	361	0.5	[37]
AA 2618 + Al_2O_3 (20 vol.%)–forged	373	453	1.3	
Al powder (10 μm) + 16 vol.% B_4C (7 μm)	160	198	18.7	[6]
Al nanoflake (0.5 μm) + 16 vol.% B_4C (7 μm)	260	364	4.8	
Al powder (31 μm) + 8.9 vol.% AlN (1 μm)	180	332	3	[20]
Al powder (1.31 μm) + 13 vol.% AlN	347	421	5	[21]
Al powder (<63 μm) + 12.7 vol.% AlN	290	474	3	
Al powder (1.31 μm) + 2.3 vol.% Al_2O_3	242	296	10	
Al powder (ball milled) + 9.6 vol.% Al_2O_3	207	345	12	
Extruded Al 1080 powder (1 μm)	243	253	8.6	Present study

+ Compression; ‡ true strain; T4 solution heat treated and naturally aged.

Several studies mentioned in Table 5 reported mechanical properties at elevated temperature (e.g., Shi et al. [2] and Li et al. [35]). However, a systematic investigation of the influence of annealing time on mechanical properties was not carried out. The results obtained in the present study also indicate a possible use of extruded Al powder at elevated temperatures. Furthermore, the material

used in the present study was produced from commercially pure Al, and no additional reinforcing particles were added. Due to the high affinity to oxidation, a thin layer of Al_2O_3 was produced during powder production and this in situ–formed Al composite material achieved mechanical properties at a relatively high level, with good high-temperature resistance to deterioration of mechanical properties.

5. Conclusions

The paper shows differences in the properties obtained after hot extrusion of Al powder in the 1 μm range. Two hot-extrusion processing routes are compared with each other. All results are discussed in light of the properties obtained after the extrusion of a conventional Al alloy of comparable chemical composition. A hot-forming study was carried out to improve the density of the extruded powder. The following conclusions can be drawn from the results obtained:

- A density of 85% was obtained after cold isostatic pressing (green pellet) when processing Al powder. After hot extrusion, this density increased to about 95%, and after hot compression, we approached 100% of the theoretical density. The conventionally cast alloy AA 1050 had a theoretical density of 100% immediately after casting.

- In an industrial environment, it was found that the use of an induction furnace to heat the green pellet to extrusion temperature was not suitable because the oxides present on the surface of the powder grains limit the heating rate. The use of gas and electric furnaces is better and our recommendation.

- A better tensile strength of the consolidated material was achieved by direct extrusion, while ductility was better when indirect extrusion was used. Although the highest values of elongation at failure were obtained in the samples of the conventional alloy AA 1050, the tensile strength in these samples was about three times lower.

- Annealing of extruded Al powder did not significantly increase the ductility, while UTS and YTS decreased slightly.

- Hot workability of powdered material is not recommended at low strain rates. Surface cracking occurred during single-hit hot-compression tests at strain rates below 0.1 s^{-1}. The yield stress of extruded Al powder was several times higher compared to the conventionally cast AA 1050 alloy. The calculated apparent activation energies for hot deformation for the material in the extruded state are 232 kJ mol^{-1} for Al 1080 powder and $158.6 \text{ kJ mol}^{-1}$ for AA 1050.

- After annealing heat treatment at 300 °C for 20 h, the apparent activation energy for hot deformation decreased more for powdered Al and was calculated to be $209.7 \text{ kJ mol}^{-1}$, while a slight change was observed for the alloy AA 1050 at 154 kJ mol^{-1}.

- Optimum hot-forming conditions are at temperatures above 550 °C and strain rates above 1 s^{-1}, based on the processing maps for strains 0.4 and 0.6.

References

1. Chelladurai, S.J.S.; Kumar, S.S.; Venugopal, N.; Ray, A.P.; Manjunath, T.C.; Gnanasekaran, S. A review on mechanical properties and wear behaviour of aluminium based metal matrix composites. *Mater. Today Proc.* **2020**. [CrossRef]
2. Shi, X.L.; Mishra, R.S.; Watson, T.J. Effect of temperature and strain rate on tensile behavior of ultrafine-grained aluminum alloys. *Mater. Sci. Eng. A* **2008**, *494*, 247–252. [CrossRef]
3. Flores-Zamora, M.I.; Estrada-Guel, I.; González-Hernández, J.; Miki-Yoshida, M.; Martínez-Sánchez, R. Aluminum–graphite composite produced by mechanical milling and hot extrusion. *J. Alloys Compd.* **2007**, *434–435*, 518–521. [CrossRef]
4. Kennedy, A.R.; Wyatt, S.M. The effect of processing on the mechanical properties and interfacial strength of aluminium/TiC MMCs. *Compos. Sci. Technol.* **2000**, *60*, 307–314. [CrossRef]
5. Chen, B.; Kondoh, K.; Li, J.S.; Qian, M. Extraordinary reinforcing effect of carbon nanotubes in aluminium matrix composites assisted by in-situ alumina nanoparticles. *Compos. Part B Eng.* **2020**, *183*, 107691. [CrossRef]
6. Kai, X.; Li, Z.; Fan, G.; Guo, Q.; Tan, Z.; Zhang, W.; Su, Y.; Lu, W.; Moon, W.-J.; Zhang, D. Strong and ductile particulate reinforced ultrafine-grained metallic composites fabricated by flake powder metallurgy. *Scr. Mater.* **2013**, *68*, 555–558. [CrossRef]
7. Balog, M.; Simancik, F.; Walcher, M.; Rajner, W.; Poletti, C. Extruded Al–Al$_2$O$_3$ composites formed in situ during consolidation of ultrafine Al powders: Effect of the powder surface area. *Mater. Sci. Eng. A* **2011**, *529*, 131–137. [CrossRef]
8. Balog, M.; Poletti, C.; Simancik, F.; Walcher, M.; Rajner, W. The effect of native Al2O3 skin disruption on properties of fine Al powder compacts. *J. Alloys Compd.* **2011**, *509*, S235–S238. [CrossRef]
9. Caballero, E.S.; Ternero, F.; Urban, P.; Cuevas, F.G.; Cintas, J. Influence of Temperature on Mechanical Properties of AMCs. *Metals* **2020**, *10*, 783. [CrossRef]
10. Caballero, E.S.; Cintas, J.; Cuevas, F.G.; Montes, J.M.; Ternero, F.; Reina, F.J.V. Synthesis and characterization of in situ-reinforced Al–AlN composites produced by mechanical alloying. *J. Alloys Compd.* **2017**, *728*, 640–644. [CrossRef]
11. Zeng, X.; Liu, W.; Xu, B.; Shu, G.; Li, Q. Microstructure and Mechanical Properties of Al–SiC Nanocomposites Synthesized by Surface-Modified Aluminium Powder. *Metals* **2018**, *8*, 253. [CrossRef]
12. Krizik, P.; Balog, M.; Illekova, E.; Svec, P.; Matko, I.; Stepanek, M.; Nosko, M.; Simancik, F. The oxidation behavior of gas-atomized Al and Al alloy powder green compacts during heating before hot extrusion and the suggested heating process. *J. Mater. Process. Technol.* **2014**, *214*, 1165–1172. [CrossRef]
13. Balog, M.; Simancik, F.; Bajana, O.; Requena, G. ECAP vs. direct extrusion—Techniques for consolidation of ultra-fine Al particles. *Mater. Sci. Eng. A* **2009**, *504*, 1–7. [CrossRef]
14. Amirkhanlou, S.; Ji, S. A review on high stiffness aluminum-based composites and bimetallics. *Crit. Rev. Solid State Mater. Sci.* **2020**, *45*, 1–21. [CrossRef]
15. Lloyd, D.J. Particle reinforced aluminium and magnesium matrix composites. *Int. Mater. Rev.* **1994**, *39*, 1–23. [CrossRef]
16. Arsenault, R.J.; Shi, N. Dislocation generation due to differences between the coefficients of thermal expansion. *Mater. Sci. Eng.* **1986**, *81*, 175–187. [CrossRef]
17. Barlow, C.Y.; Hansen, N. Dislocation configurations in metal-matrix composites correlated with numerical predictions. *Acta Metall. Mater.* **1995**, *43*, 3633–3648. [CrossRef]
18. Dai, L.H.; Liu, L.F.; Bai, Y.L. Formation of adiabatic shear band in metal matrix composites. *Int. J. Solids Struct.* **2004**, *41*, 5979–5993. [CrossRef]
19. Fleck, N.A.; Ashby, M.F.; Hutchinson, J.W. The role of geometrically necessary dislocations in giving material strengthening. *Scr. Mater.* **2003**, *48*, 179–183. [CrossRef]
20. Yu, P.; Balog, M.; Yan, M.; Schaffer, G.B.; Qian, M. In situ fabrication and mechanical properties of Al–AlN composite by hot extrusion of partially nitrided AA6061 powder. *J. Mater. Res.* **2011**, *26*, 1719–1725. [CrossRef]
21. Balog, M.; Krizik, P.; Yan, M.; Simancik, F.; Schaffer, G.B.; Qian, M. SAP-like ultrafine-grained Al composites dispersion strengthened with nanometric AlN. *Mater. Sci. Eng. A* **2013**, *588*, 181–187. [CrossRef]

22. Poletti, C.; Balog, M.; Simancik, F.; Degischer, H.P. High-temperature strength of compacted sub-micrometer aluminium powder. *Acta Mater.* **2010**, *58*, 3781–3789. [CrossRef]

23. Balog, M.; Krizik, P.; Bajana, O.; Hu, T.; Yang, H.; Schoenung, J.M.; Lavernia, E.J. Influence of grain boundaries with dispersed nanoscale Al2O3 particles on the strength of Al for a wide range of homologous temperatures. *J. Alloys Compd.* **2019**, *772*, 472–481. [CrossRef]

24. Jonas, J.J.; Sellars, C.M.; Tegart, W.J.M. Strength and structure under hot-working conditions. *Metall. Rev.* **1969**, *14*, 1–24. [CrossRef]

25. Kugler, G.; Knap, M.; Palkowski, H.; Turk, R. Estimation of Activation Energy for Calculating the Hot Workability Properties of Metals. *Metalurgija* **2004**, *43*, 267–272.

26. Bombac, D.; Brojan, M.; Tercelj, M.; Turk, R. Response to hot deformation conditions and microstructure development of nimonic 80a superalloy. *Mater. Manuf. Process.* **2009**, *24*, 644–648. [CrossRef]

27. Mehrer, H.; Bakker, H.; Bonzel, H.P.; Bruff, C.M.; Dayananda, M.A.; Gust, W.; Horvath, J.; Kaur, I.; Kidson, G.V.; LeClaire, A.D.; et al. Diffusion in Solid Metals and Alloys/Diffusion in festen Metallen und Legierungen. In *Landolt-Börnstein: Numerical Data and Functional Relationships in Science and Technology—New Series/Condensed Matter*; Springer: Berlin/Heidelberg, Germany, 1990; ISBN 9783540508861.

28. Prasad, Y.V.R.K.; Rao, K.P.; Sasidhara, S. (Eds.) *Hot Working Guide: A Compendium of Processing Maps*, 2nd ed.; ASM International: Materials Park, OH, USA, 2015; ISBN 9781627080927.

29. Prasad, Y.V.R.K. Processing maps: A status report. *J. Mater. Eng. Perform.* **2003**, *12*, 638–645. [CrossRef]

30. Kubota, M. Properties of nano-structured pure Al produced by mechanical grinding and spark plasma sintering. *J. Alloys Compd.* **2007**, *434–435*, 294–297. [CrossRef]

31. Gubicza, J.; Dirras, G.; Szommer, P.; Bacroix, B. Microstructure and yield strength of ultrafine grained aluminum processed by hot isostatic pressing. *Mater. Sci. Eng. A* **2007**, *458*, 385–390. [CrossRef]

32. Zhang, W.; Chai, D.; Ran, G.; Zhou, J. Study on microstructure and tensile properties of in situ fiber reinforced aluminum matrix composites. *Mater. Sci. Eng. A* **2008**, *476*, 157–161. [CrossRef]

33. Song, M.; He, Y. Effects of die-pressing pressure and extrusion on the microstructures and mechanical properties of SiC reinforced pure aluminum composites. *Mater. Des.* **2010**, *31*, 985–989. [CrossRef]

34. Choi, H.J.; Lee, S.W.; Park, J.S.; Bae, D.H. Tensile behavior of bulk nanocrystalline aluminum synthesized by hot extrusion of ball-milled powders. *Scr. Mater.* **2008**, *59*, 1123–1126. [CrossRef]

35. Li, Z.J.; Wang, L.D.; Fei, W.D. Effect of interfacial Bi2O3 coating on compressive deformation behavior of aluminum borate whisker-reinforced aluminum composite at elevated temperature. *Mater. Sci. Eng. A* **2007**, *447*, 314–318. [CrossRef]

36. Badini, C.; La Vecchia, G.M.; Fino, P.; Valente, T. Forging of 2124/SiCp composite: Preliminary studies of the effects on microstructure and strength. *J. Mater. Process. Technol.* **2001**, *116*, 289–297. [CrossRef]

37. Ceschini, L.; Minak, G.; Morri, A. Forging of the AA2618/20vol.% Al2O3p composite: Effects on microstructure and tensile properties. *Compos. Sci. Technol.* **2009**, *69*, 1783–1789. [CrossRef]

38. Fan, G.J.; Wang, G.Y.; Choo, H.; Liaw, P.K.; Park, Y.S.; Han, B.Q.; Lavernia, E.J. Deformation behavior of an ultrafine-grained Al–Mg alloy at different strain rates. *Scr. Mater.* **2005**, *52*, 929–933. [CrossRef]